



Response to Ballistic Impact of Alumina-UHMWPE Composites

André Ben-Hur da Silva Figueiredo^{a*}, Édio Pereira Lima Júnior^a, Aaelson Vieira Gomes^a,

Gabriel Burlandy Mota de Melo^a, Sergio Neves Monteiro^a, Ronaldo Sergio de Biasi^a

^aSeção de Engenharia Mecânica e de Materiais, Instituto Militar de Engenharia, Praça General Tibúrcio, 80, 22290-270, Rio de Janeiro, RJ, Brasil

Received: October 24, 2017; Revised: May 23, 2018; Accepted: July 05, 2018

The response to ballistic impact of alumina-ultra high molecular weight polyethylene (UHMWPE) composites with different relative concentrations of alumina was investigated. The impact tests were carried out at subsonic speed using a compressed air system. The results showed that the depth of penetration (DOP) in a Medium Density Fiberboard (MDF) bulkhead protected by a disk of the composite decreased with increasing concentration of alumina in the composite. Scanning electron microscopy (SEM) images of composites with 80 %, 85 % and 95 % alumina showed transgranular, intergranular and ductile fracture mechanisms.

Keywords: *ballistic shielding, ballistic impact, alumina-UHMWPE composite.*

1. Introduction

In the beginning of the 21st century, local and regional conflicts are a sad reality. In this scenario, attack and defense equipment is a flourishing field of research.

The current bulletproof personal protection vests use a single layer of aramid fabric¹. This protection, however, is limited to relatively low impact velocities. Protection against heavier armament requires a multilayered armor system (MAS)². Conventional MAS have a ceramic front layer which erodes the projectile tip. This mechanism of energy dissipation involves not only fragmentation of the projectile but also fragmentation of the ceramic.

The main ceramic materials used in ballistic protection are alumina (Al₂O₃), silicon carbide (SiC) and boron carbide (B₄C). Alumina has been widely used for all kinds of protection because of its hardness, abrasion resistance and chemical inertia. However, its low flexural strength and low fracture toughness mean that the use of pure alumina for protection may lead to catastrophic failure. Moreover, its high density limits its use in applications where weight is crucial, such as bulletproof vests³⁻⁶.

The purpose of this work was to investigate the properties of alumina-UHMWPE composites in which UHMWPE is used to decrease density and increase flexural strength and fracture toughness, making the shield more suitable for personal protection and avoiding fracture after the first shot^{7,8}. There is also an economic factor involved, since the composite is prepared at a relatively low temperature, 230°C, while pure alumina must be prepared sintering alumina powder at high temperatures, of the order of 1400°C, a more expensive procedure⁹.

2. Materials and Methods

2.1 Materials

The materials used were 60-mesh Alundum powder with 9.25 Moh hardness (Fisher Scientific), UHMWPE Mipelon PM-200 powder with 10 μm average diameter (Mitsui Chemicals) and 1 inch thick MDF (Arauco do Brasil).

2.2 Sample preparation

Composites with different alumina-UHMWPE mass ratios were prepared by mechanical mixing for 10 min and labeled A20, A40, A60, A80, A85, A90 and A95, where 20, 40, etc. is the alumina mass concentration in percent. Mixing was performed using a Britânia mechanical mixer. No solvent was used.

The samples were produced in the shape of discs 5 mm thick and 51 mm in diameter. The discs were pressed at 230°C for 10 minutes under a force of 90 kN. The A00 and A100 samples are, respectively, pure UHMWPE and pure alumina sintered using a previously described route⁹.

2.3 Characterization

For the ballistic tests, a Gunpower SSS air rifle was used with a noise suppressor Padrão Armas. The projectile was a 22 gauge lead shot with an estimated mass of 3.3 g. The impact speed was measured using an Air Chrony ballistic chronograph model MK3 with a precision of 0.15 m/s.

After the ballistic tests, images of the composites with 80 %, 85 % and 95 % alumina were obtained in a FEI Quanta FEG 250 SEM.

2.4 Ballistic tests

In the ballistic tests, the air rifle was positioned 5 m away from the target, consisting of a composite disk attached with

*e-mail: abenhur@ime.eb.br

adhesive tape to an MDF plate and aligned perpendicularly to the rifle.

The noise suppressor was used to increase the stability of the projectile at the exit of the air rifle by reducing the swirling caused by the exhaust.

MDF plates were used as bulkheads because MDF is a homogeneous material, flat and dense, not having the grain of solid wood.

The ballistic chronograph was placed 10 cm from the exit of the noise suppressor.

Figure 1 shows the result of a typical shot.

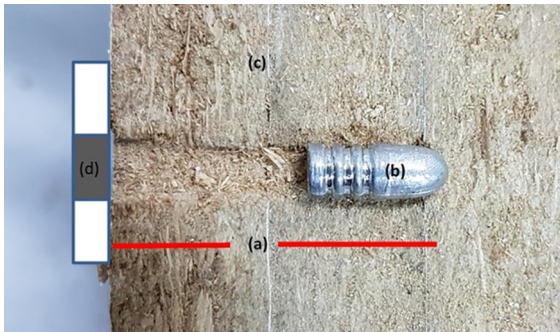


Figure 1. Result of a typical shot. (a) Depth of penetration (DOP) measured from the surface of the bulkhead to the tip the projectile; (b) projectile; (c) MDF bulkhead; (d) composite disk.

For ogival projectiles, the depth of penetration (DOP) in the bulkhead depend on the projectile mass and the impact speed¹⁰⁻¹⁵. Taking into account the fact that in the case of personal protection weight may be an important factor, one may define a figure of merit given by the following equation:

$$FM = 100 / (DOP \times M_s)$$

where M_s is the sample mass.

3. Results and Discussion

3.1 Ballistic tests

All shots completely penetrated the disk. Two shots were made in each experiment and five experiments were performed for each composition. The results are shown in Fig. 2 for A00, A20, A40, A60 and A80 samples.

Table 1 shows the projectile mass, the average impact speed (v), the depth of penetration (DOP), the sample mass (M_s) and the figure of merit (FM) for each composition. Since the projectile mass and the impact speed were about the same for all tests, the results could be directly compared. Except for A100 (pure alumina), with is included only for comparison, the samples with the highest figure of merit were A00 and A90. This suggests that the adhesion between alumina particles and UHMWPE is very weak.

Figure 3 shows the dependence of DOP on alumina concentration. The composite with the lowest alumina concentration (A20) has a value of DOP larger than that of pure UHMWPE, probably due to the fact that a small addition of alumina introduces defects in UHMWPE without contributing significantly to increase its resistance to penetration. For larger concentrations of alumina, increasing the alumina concentration increases the shear thickening

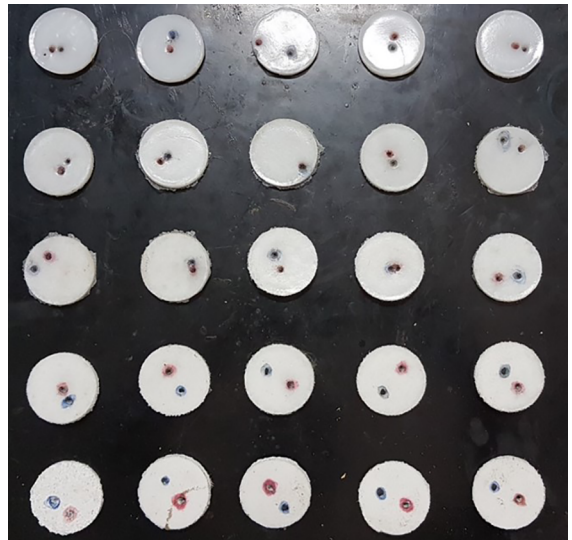


Figure 2. A00, A20, A40, A60 and A80 samples arranged in top-down rows, after the ballistic tests

Table 1. Average results of the ballistic tests.

SAMPLE	M_p (g)	v (m/s)	DOP (mm)	M_s (g)	FM ($\text{mm}^{-1}\text{g}^{-1}$)
A00	3.23 ± 0.08	245.56 ± 2.14	19.83 ± 0.94	9.09 ± 0.20	0.55 ± 0.01
A20	3.23 ± 0.09	243.69 ± 1.69	21.16 ± 1.11	11.00 ± 0.33	0.43 ± 0.01
A40	3.23 ± 0.10	245.13 ± 1.29	19.63 ± 0.99	13.89 ± 0.23	0.37 ± 0.01
A60	3.23 ± 0.08	246.35 ± 1.25	14.49 ± 1.12	18.88 ± 0.64	0.37 ± 0.01
A80	3.24 ± 0.12	244.65 ± 1.72	6.89 ± 0.90	32.94 ± 0.32	0.44 ± 0.01
A85	3.17 ± 0.25	255.97 ± 2.13	6.75 ± 0.97	34.15 ± 1.12	0.43 ± 0.01
A90	3.25 ± 0.14	249.80 ± 1.46	4.25 ± 0.97	44.47 ± 1.60	0.53 ± 0.03
A95	3.23 ± 0.10	259.95 ± 0.89	3.85 ± 1.30	56.24 ± 0.10	0.46 ± 0.03
A100	3.26 ± 0.08	243.67 ± 1.01	1.10 ± 0.31	62.18 ± 2.79	1.46 ± 0.21

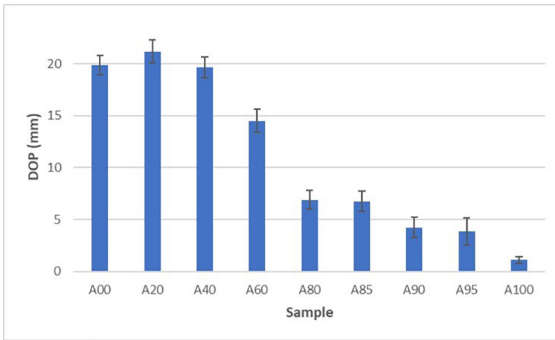


Figure 3. Dependence of DOP on alumina concentration.

effect with the appearance of hydroclusters during the collision^{16,17}. For alumina concentrations above 60 %, one observes a significant decrease in DOP, which is probably due to the increased contribution of the UHMWPE crystallized region around the particles due to a decrease of the distance between the particles¹⁶.

3.2 SEM images of alumina powder and samples A80, A85 and A95

Figure 4 is a SEM Image of the alumina powder, showing the irregular shape of the particles, which improves the stiffness of the composites, since the aggregates formed by these particles have a low density and contain continuous pores that are filled with UHMWPE. The same phenomenon has been observed in fumed silica¹⁷.

Figure 5 shows the distal face of an A80 sample; the crater formed by the projectile impact is clearly seen, surrounded by a small concussion zone.

Figure 6a is a SEM image of the impact region of an A80 sample, showing a transgranular fragile fracture and a ductile region of UHMWPE. The surface of the sample has small voids, which are attributed to a low UHMWPE content.

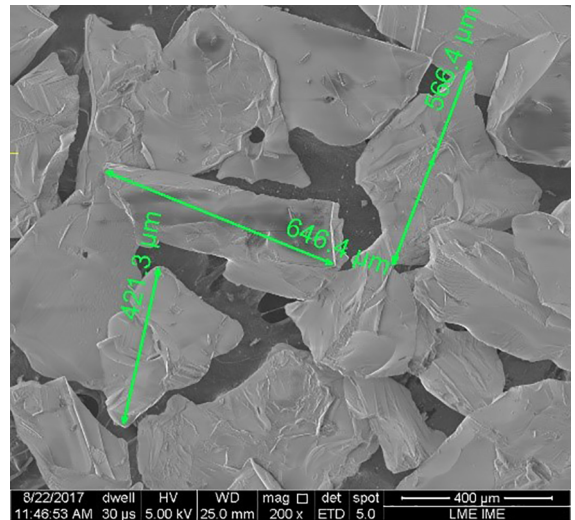


Figure 4. SEM image of the alumina powder.

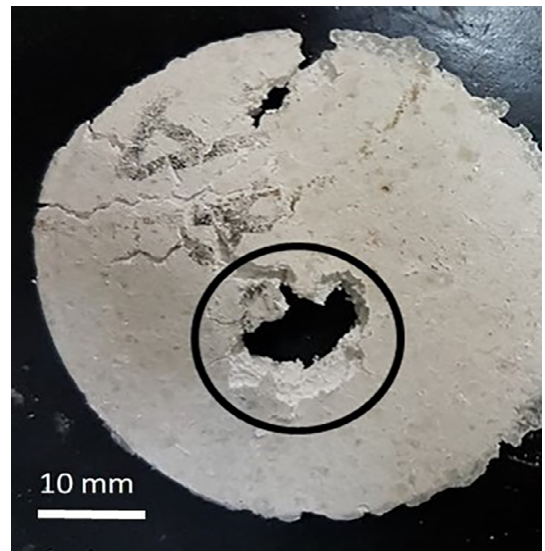


Figure 5. Optical image of the distal face of an A80 sample, showing the crater formed by impact.

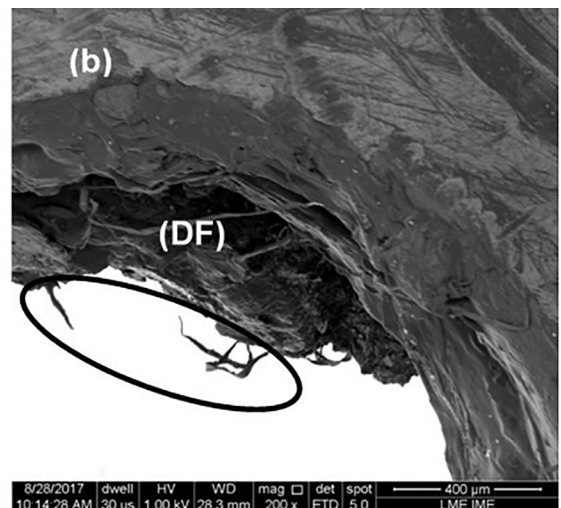
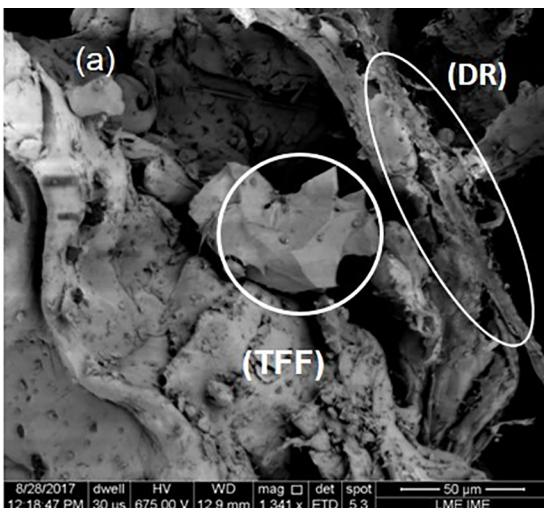


Figure 6. SEM images (a) of sample A80 with transgranular fragile fracture (TFF) and ductile region (DR); (b) of sample A85 with ductile fracture (DF).

Figure 6b is a SEM image of sample A85, showing a ductile fracture of UHMWPE that contributes to increase the tenacity^{7,8}.

Figure 7 is a SEM image of an A95 sample, showing alumina particles with irregular shapes and high porosity. It shows transgranular fracture and reduced participation of ductile fracture in energy absorption.

Figure 8a is the SEM image of an A95 sample, showing that a good quality interface is produced, that is, a good contact (without voids) between matrix and reinforcement is observed; a transgranular fracture is clearly seen. Figure 8b shows a crack in another A95 sample, attributed to more than one mechanism.

Figure 9 shows the SEM image of an A95 sample with primarily a transgranular fracture and a ductile fracture of UHMWPE.

Although samples A100 had the lowest penetration depth, they were shattered by the first shot.

4. Conclusions

The samples with the highest figure of merit were samples A00 and A90, suggesting the absence of interfacial adhesion between the alumina particles and the UHMWPE matrix.

Composition A90 (90 % alumina and 10 % UHMWPE) was the one that presented best performance in terms of weight and penetration depth.

SEM images of samples A80, A85 and A95 showed several modes of energy absorption of the projectile impact. The primary mechanism of energy absorption was transgranular fracture after hydroclusters form in the sample, followed by ductile fracture of partially crystallized UHMWPE.

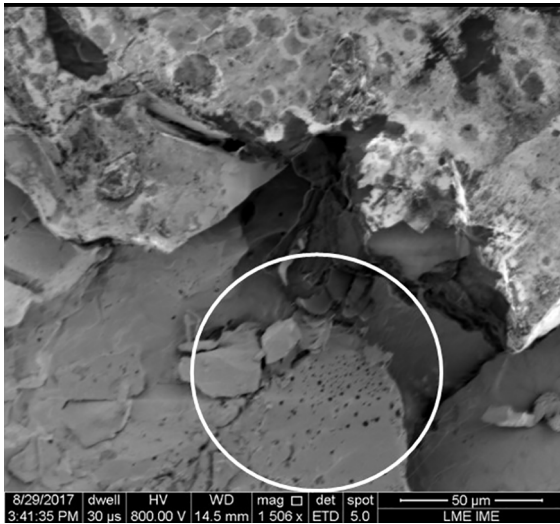


Figure 7. SEM image of sample A95, showing the porosity of alumina particles.

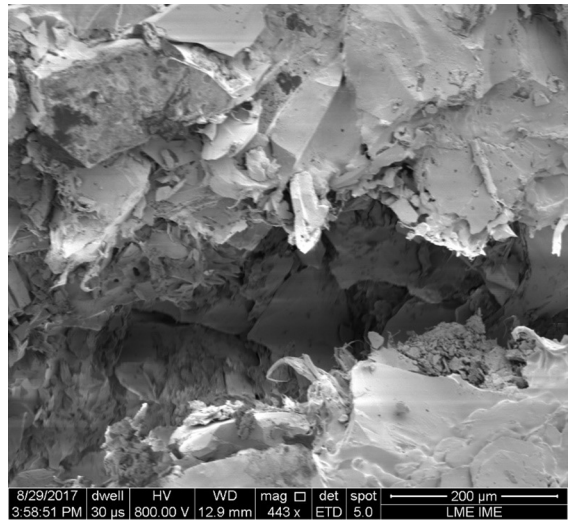


Figure 9. SEM image of a section of the crack of Figure 8b, showing participation of all mechanisms in the crack

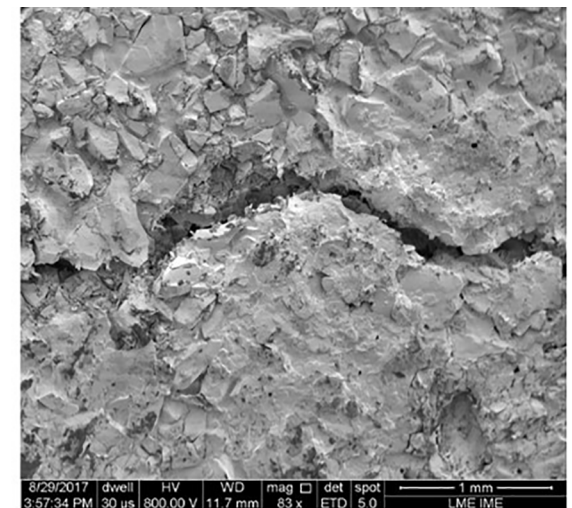
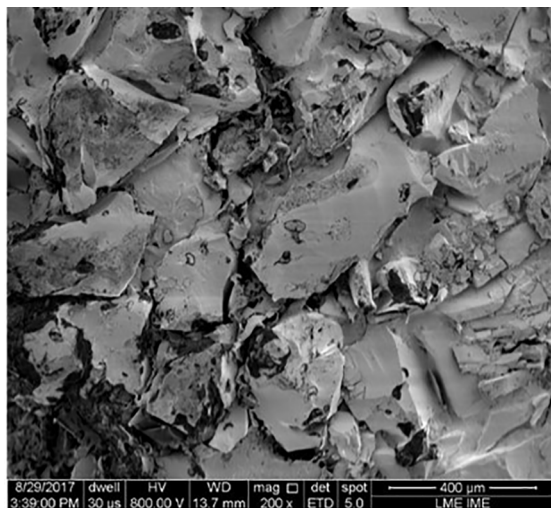


Figure 8. SEM images of A95 samples, showing (a) a transgranular fracture and (b) a crack.

5. References

1. Cavallaro PV. *Soft Body Armor: An Overview of Materials, Manufacturing, Testing, and Ballistic Impact Dynamics*. NUWC-NPT Technical Report 12,057. Newport: Naval Undersea Warfare Center Division; 2011.
2. Luz FS, Lima Junior EP, Louro LHL, Monteiro SN. Ballistic Test of Multilayered Armor with Intermediate Epoxy Composite Reinforced with Jute Fabric. *Materials Research*. 2015;18(Suppl 2):170-177.
3. Medvedovski E. Ballistic performance of armor ceramics: Influence of design and structure. Part I. *Ceramics International*. 2010;36(7):2103-2115.
4. Medvedovski E. Ballistic performance of armor ceramics: Influence of design and structure. Part 2. *Ceramics International*. 2010;36(7):2117-2127.
5. Medvedovski E. Lightweight ceramic composite armor system. *Advances in Applied Ceramics*. 2006;105(5):241-245.
6. Louro LHL, Meyers MA. Effect of stress state and microstructural parameters on impact damage of alumina-based ceramics. *Journal of Materials Science*. 1989;24(7):2516-2532.
7. Coutinho FMB, Mello IL, Santa Maria LC. Polietileno: Principais Tipos, Propriedades e Aplicações. *Polímeros*. 2003;13(1):1-13.
8. Senatov FS, Gorshenkov MV, Tcherdyntsev VV, Kaloshkin SD, Sudarchikov VA. Fractographic analysis of composites based on ultra high molecular weight polyethylene. *Composites Part B: Engineering*. 2014;56:869-875.
9. Trindade W, Gomes AV, Louro LHL. Elaboração de uma Nova Rota de Eliminação de Ligante da Cerâmica de Alumina. *Revista Militar de Ciência & Tecnologia*. 2013;4:71-79.
10. Carlucci DE, Jacobson SS. *Ballistics: Theory and Design of Guns and Ammunition*. Boca Raton: CRC; 2008. 496 p.
11. Azevedo G, Aragão JCT. *Apontamentos sobre Balística*. Rio de Janeiro; 2010.
12. Anderson CE Jr. Analytical models for penetration mechanics: A review. *International Journal of Impact Engineering*. 2017;108:3-26.
13. Shokrieh MM, Javadpour GH. Penetration analysis of a projectile in ceramic composite armor. *Composite Structures*. 2008;82(2):269-276.
14. Backman ME, Goldsmith W. The mechanics of penetration of projectiles into targets. *International Journal of Engineering Science*. 1978;16(1):1-99.
15. Jonas GH, Zukas JA. Mechanics of penetration: Analysis and experiment. *International Journal of Engineering Science*. 1978;16(11):879-903.
16. Galindo-Rosales FJ, Rubio-Hernández FJ, Sevilla A. An apparent viscosity function for shear thickening fluids. *Journal of Non-Newtonian Fluid Mechanics*. 2011;166(5-6):321-325.
17. Ding J, Tracey PJ, Li W, Peng G, Whitten PG, Wallace GG. Review on shear thickening fluids and applications. *Textiles and Light Industrial Science and Technology*. 2013;2(4):161-173.